ORNL/TM-2024/3609

Design and Construction of a 75-Watt Electrically Heated Bismuth-Telluride Thermoelectric Generator for Demonstration and Model Validation

Nolan Goth
Daniel Orea
Darren Loposser
Hsin Wang
Trevor Parker
Brad Johnson

Approved for public release.
Distribution is unlimited.

October 2024

OAK RIDGE National Laboratory

ORNL IS MANAGED BY UT-BATTELLE LLC FOR THE US DEPARTMENT OF ENERGY

ORNL/TM-2024/3609

Nuclear Energy and Fuel Cycle Division

DESIGN AND CONSTRUCTION OF A 75-WATT ELECTRICALLY HEATED BISMUTH-TELLURIDE THERMOELECTRIC GENERATOR FOR DEMONSTRATION AND MODEL VALIDATION

Nolan Goth
Daniel Orea
Darren Loposser
Hsin Wang
Trevor Parker
Brad Johnson

October 14, 2024

Prepared by
OAK RIDGE NATIONAL LABORATORY
Oak Ridge, TN 37831
managed by
UT-BATTELLE LLC
for the
US DEPARTMENT OF ENERGY
under contract DE-AC05-00OR22725

CONTENTS

LIST OF FIGURES

LIST OF TABLES

LIST OF ABBREVIATIONS

AM	additively manufactured
BiTe	bismuth-telluride
ETG	electrically heated thermoelectric generator
HDB	heat distribution block
ORNL	Oak Ridge National Laboratory
PLC	programmable logic controller
RTG	radioisotope thermoelectric generator
TEM	thermoelectric module

ABSTRACT

Radioisotope thermoelectric generators (RTGs) serve a crucial role providing thermal and electrical energy for long-duration missions often in extreme environments such as the arctic, marine, and outer space biomes. Many current designs still rely on geometries and materials dating back to the 1960s. However, the advent of additive manufacturing presents an opportunity to revolutionize RTG design by allowing for the creation of intricate geometries that optimize heat transfer pathways through the thermoelectric legs. Significant advancements in materials research and engineering since the inception of the RTG offer new possibilities for enhancing device performance through the manipulation of grain morphology and material properties.The Nuclear Battery Initiative at Oak Ridge National Laboratory (ORNL) is focused on innovating in and advancing this field by applying state-of-the-art fabrication and modeling capabilities. These multiphysics computational models couple the heat transfer modes of conduction, convection, and radiation with systems of equations relevant to thermoelectric devices for Seebeck, Thompson, and Joule effects. The predictive capability enables quantification of the electrical response of the thermoelectric generator based on the heat source power input, heat rejection, and the external electrical load on the system. ORNL has designed and constructed two simple electrically heated thermoelectric generators for demonstration and model validation. The functional requirements and design of each are discussed in this paper.

1. INTRODUCTION

Radioisotope thermoelectric generators (RTGs) serve a crucial role providing thermal and electrical energy for long-duration missions often in extreme environments such as the arctic, marine, and outer space biomes. Generating electrical energy on the principle of the Seebeck effect, RTGs produce electricity by achieving temperature differentials across dissimilar materials in contact. Although traditional thermoelectric generators typically exhibit modest efficiencies ranging from 3% to 7% [1, 2], their appeal lies in their exceptional reliability due to a lack of moving parts by using the thermal energy produced by radioactive decay to establish the necessary temperature gradient for electrical power generation. RTGs have played pivotal roles in numerous space missions, providing continuous and dependable power for instruments aboard spacecraft such as the Mars rovers ([3]) and the Cassini-Huygens Saturn orbiter ([4]).

Although RTGs have been integral to space and subsea missions for decades [5, 6], there has been a notable stagnation in the advancement of their design, with past and ongoing efforts to repurpose or dispose of previously developed RTGs [7]. Many current designs still rely on geometries and materials dating back to the 1960s. However, the advent of additively manufactured (AM) presents an opportunity to revolutionize RTG design by allowing for the creation of intricate geometries that optimize heat transfer pathways through the thermoelectric legs [8]. Significant advancements in materials research and engineering since the inception of the RTG offer new possibilities for enhancing device performance through the manipulation of grain morphology and material properties. The Nuclear Battery Initiative at Oak Ridge National Laboratory (ORNL) is focused on innovating in and advancing this field by applying state-of-the-art fabrication and modeling capabilities.

Leveraging model-based systems engineering methods and established numerical tools within software packages, models of thermoelectric modules (TEMs) and RTG systems are being investigated at ORNL to topologically optimize the design for AM. These multiphysics computational models couple the heat transfer modes of conduction, convection, and radiation with systems of equations relevant to thermoelectric devices for Seebeck, Thompson, and Joule effects. The predictive capability enables quantification of the electrical response of the TEM based on the heat source power input, heat rejection, and the external

electrical load on the system. TEMs can present challenges related to modeling because of the complexity that arises from thermal and electrical feedback, which affect physical parameters such as thermal conductivity, thermal resistance, and Seebeck coefficient. Quantifying the physical properties of TEMs is nontrivial, with significant effort in the past to measure transport properties [9, 10]. Comparison and validation against experimental data is an important step to ensure the proper physics is being captured in the model.

The use of electric heaters to simulate nuclear fuel is a common practice in nuclear engineering [11, 12]. The thermal and stress performance of nuclear systems can be evaluated using nonnuclear test platforms. An electrically heated test bed can provide input regarding system components while reducing the time, cost, and risk associated with the complexities of a nuclear-fueled systems. In the case of a RTG, the heat-generating radioisotope can be simulated using an electrical heater to rapidly test and iterate through designs before introducing a sealed nuclear fuel heat source.

Therefore, ORNL has designed and constructed two simple electrically heated thermoelectric generators (ETGs) for demonstration and model validation. The demonstration ETG unit was assembled using a 75 W cartridge heater to provide heat to two separate bismuth-telluride (BiTe) TEMs. Each TEM is paired with a heat sink configuration consisting of a mounting plate, multiple heat pipes, a large heat sink geometry, and cooling fans. The heat source and heat distribution system are surrounded by two types of insulating material: rigid min-k and flexible silica. The configured ETG is packaged inside a thin aluminum shell, which is secured inside a protective case for travel. The demonstration unit aids in understanding the compact size, reliability, and functionality of an RTG to deliver electrical power. Exhibitions of the ETG unit have demonstrated its capability to switch between supplying power to its own cooling fans and recharging a battery pack of a $1/40$ scaled submersible vehicle. A second and fully instrumented ETG was constructed for the purpose of generating data for model validation and testing of various TEM designs. This unit can control and record the system temperature, voltage, current, and electrical power, along with the ability to vary the TEM circuit load resistance.

2. DESIGN

Two experimental nonnuclear RTGs, hence referred to as ETGs, were designed and assembled to generate thermal and electrical performance data for numerical model comparison and validation. The ETGs included the main components of an RTG, with the exception of the radioisotope heat source. The design process consisted of research, establishing requirements, feasibility studies, concept generation, preliminary design, and final design. Research consisted of literature reviews of RTG designs to increase understanding of legacy and modern conceptual design spaces.

The establishment of requirements began by defining lists of functional and nonfunctional requirements. The primary requirement was to convert electrical energy into thermal energy and back into electrical energy. Finned heat sinks were selected to reject thermal energy to the surrounding air. Temperatures were selected to ensure the TEMs would operate at near their maximum performance level, such as: (1) achieving a hot shoe temperature of at least 150°C, (2) achieving a cold shoe temperature of at least 50°C, and (3) achieving a temperature difference of at least 100°. To accelerate the design and construction processes, the use of commercial-off-the-shelf components was prioritized. The ETG dimensions were restricted at or below $8 \times 8 \times 6$ in. (L × W × H). The ETG needed to supply thermal power to two TEMs. A temperature-controlled proportional-integral loop was required to control the electrical heater power via the TEM hot shoe temperature. The ETG electrical power output was required to drive the cooling fans on the heat sinks. Safety hazards were minimized by using sufficient insulation to maintain enclosure top, side, and bottom surfaces below 50°C. Also, the contact temperature resistances were reduced by using boron nitride paste at high-temperature interfaces and by using silver paste at low-temperature interfaces.

Feasibility studies consisted of approximate hand calculations and use of existing subject matter expertise at ORNL. Concept generation took place through brainstorming with a group of people with diverse technical backgrounds. The preliminary design was matured through an iterative process using finite-volume computational modeling within STAR-CCM+ 18.02.010, a state-of-the-art multiphysics software package developed by Siemens. This software has an extensive user base, a set of validation studies, and is compliant with the American Society of Mechanical Engineers' Nuclear Quality Assurance 1 standard.

Figure 1 presents the primary components of the ETG final design. Primary components included one electrical strip heater (McMaster # 3576K63), one machined copper alloy 110 heat distribution block (HDB), two BiTe TEMs (Marlow TG12-2.5-01LS), two heat sinks (Noctua NH-L9x65), machinable rigid insulation (Min-k TE 1400), flexible insulation (ZRCI Type SB-2000), and one aluminum enclosure.

Figure 2 presents the assembly process of the ETG. Further detail is provided in Appendix A. The strip heater was mounted onto the bottom of the HDB using 5/16–18 in. bolts, Belleville conical washers, and regular washers. The bolts on the same side as the wire terminals were fully tightened, while the bolts opposite of the terminals were fastened slightly past hand-tight to allow for elongated thermal expansion of the heater. Two square pedestals machined into the copper block directed heat flow to the TEMs. The TEMs were compressed between the copper pedestal and the heat sinks. Boron nitride thermal paste was applied between the strip heater and the bottom of the copper block, as well as between the copper pedestal and the hot shoe of the TEMs. Noctua NT-H1 thermal paste was used between the TEM cold shoe and heat sinks. Each heat sink consisted of four parallel heat pipes, with the evaporator ends connected by a common hot plate, and the condenser ends with fins. The assembly was enclosed in an aluminum box lined with Min-K and ZRCI Type SB-2000 insulation.

The computational domain consisted of solid regions to represent the strip heater element, strip heater sheath, HDB, and the TEMs and their subdomains (hot shoes, hot copper bridge interconnects, legs, cold

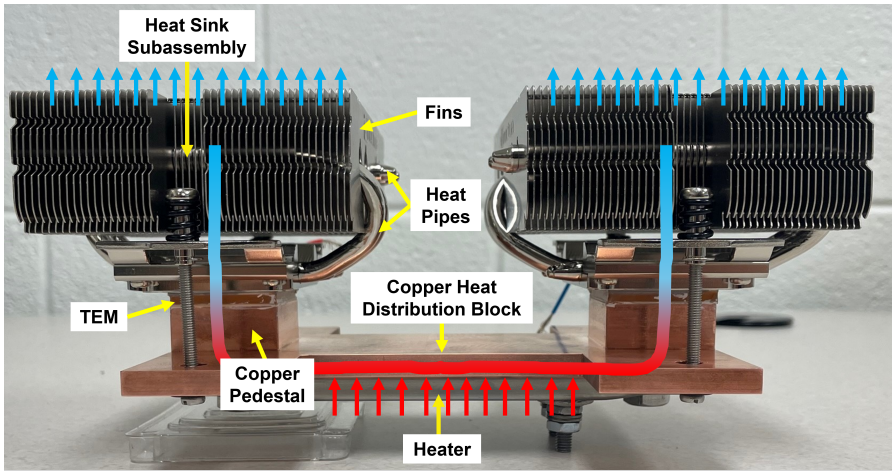

Figure 1. Overview of the final ETG design showing the heater, heat distribution block, TEMs, and heat sink configuration without enclosure or insulation (red-blue line represents the temperature gradient and heat path).

copper bridge interconnects, and hot shoes). Figure 3 presents the primary components. The forced convection heat sinks, associated heat pipes, and natural circulation around the aluminum enclosure were neglected at this time. All boundary and interfacial conditions are specified in Table 1 for each region.

The electrical strip heater was modeled as two simplified solid regions, namely the heater element and heater sheath. The physical inner heating element consists of helically wound nickel-chrome resistance wire coils. These coils are distributed throughout a MgO ceramic insulator. The ceramic block attempts to achieve a spatially uniform heat flux along the heater mounting surface. The interstitial volume between the wire coils and ceramic block is packed MgO powder to increase thermal conductivity and dielectric strength. The computational heater is composed of a rectangular prism MgO heater element with an outer encapsulating rectangular prism UNS S30400 sheath.

The design phase of this effort needed to be limited to two weeks to accelerate the construction of the Demonstration Unit (Section 3) and the Validation Unit (Section 4). Therefore, the physics models were maintained as simple as possible by activating only internal thermal conduction and convective boundary physics. At this time, no electrical physics were implemented. Also, the thermoelectric physics comprising the Seebeck Effect, Thompson Effect, and Joule Heating were neglected. Instead, a decoupled set of hand calculations using the TEM manufacturer's performance specifications were made during the design process.

The TEM thermal sink was also simplified by defining it as a set of surface temperatures at the cold shoes, and a set of convective heat transfer coefficients were applied to the six surfaces (top, sides, and bottom) of the aluminum enclosure. This approach avoided the computational complexities associated with two-phase conjugate heat transfer within eight heat pipes and with rigid body motion or moving reference frame methodologies to simulate fan rotation, forced convective flow, and natural convective flow. A decoupled set of hand calculations using the heat sink manufacturer's performance specifications were made during the design process.

Table 2 contains the material properties used in this effort. Polynomial equations were used to represent the temperature-dependent thermal conductivity in each material. The material densities and specific heat capacities were specified as constants.

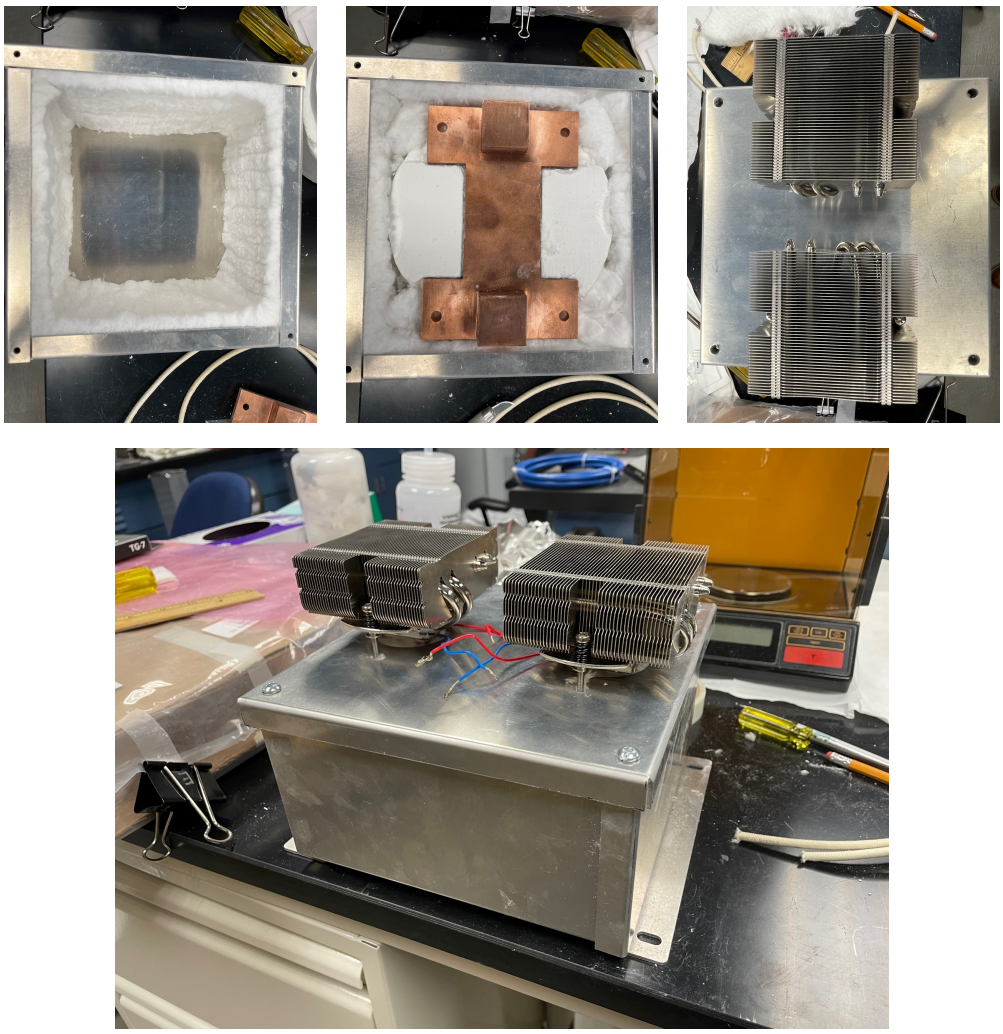

Figure 2. Assembly of the ETG.

For the solid regions, 3D gradients, a steady time scheme, and segregated solid energy models were specified. The solid energy equation is given by

$$\frac{d}{dt}\iiint_V \rho_s c_{p,s} T \, dV + \oint_A \rho c_{p,s} T \boldsymbol{v_s} \cdot d\boldsymbol{a} = -\oint_A \dot{\boldsymbol{q}}_{\boldsymbol{s}}'' \cdot d\boldsymbol{a} + \iiint_V S_u dV \ , \tag{1}$$

where ρ_s is the solid density, $c_{p,s}$ is the solid specific heat capacity, T is the solid temperature, $\dot{\boldsymbol{q}}_{\boldsymbol{s}}''$ is the solid heat flux vector, $\boldsymbol{v_s}$ is the solid convective velocity, and S_u is the solid volumetric heat source.

Fully conformal meshes were generated using a singular polyhedral meshing operation. First, a surface remesher performed surface vertex retessellation of the 3D model to optimize surface faces based on the target edge length and proximity refinements. Second, a tetrahedral volumetric mesh was generated from the remeshed surface. Third, a polyhedral mesh was generated from the underlying tetrahedral mesh.

This modeling and simulation effort provided valuable predictive capabilities that aided and accelerated the conceptual design. With an internal heat source of 75 W, 50°C cold shoe temperature, and approximate convective boundary conditions, the model predicted that each TEM hot shoe would reach 208°C and would need 32 W of thermal power. This equated to a heat flux of 35.5 kW m^{-2} per TEM. The model

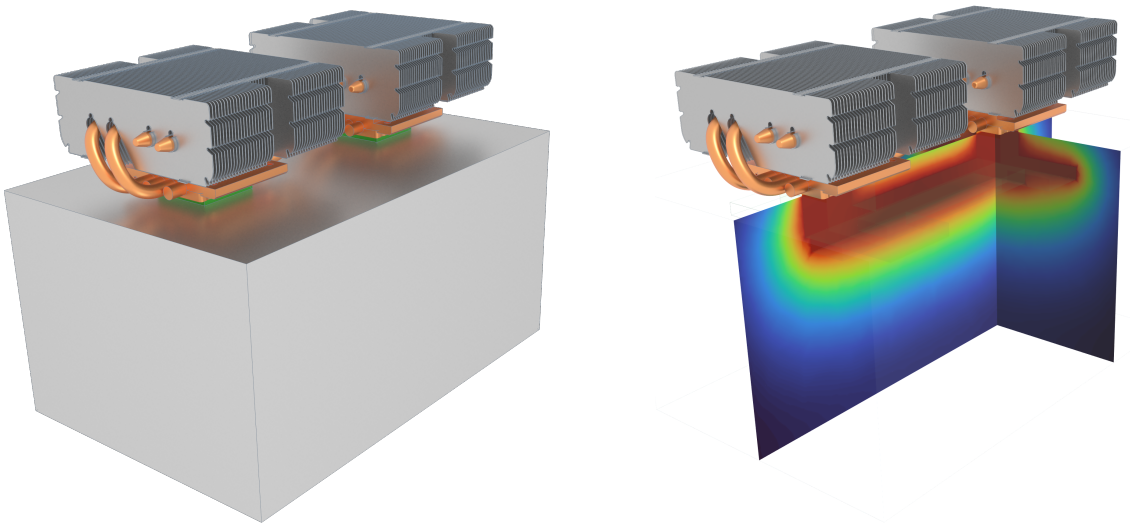

Figure 3. Computational domain of the ETG within its aluminum enclosure.

was used to predict that expected heater temperatures would be significantly less than the design limit of 650°C. It also aided in sizing the insulation thickness to ensure all exterior surfaces were below the 50°C limit to avoid damaging any table surface during demonstration exercises and to minimize the safety hazard of exposed hot surfaces. Figure 4 presents temperature contours along the midplane of the entire ETG and a close-up of a TEM.

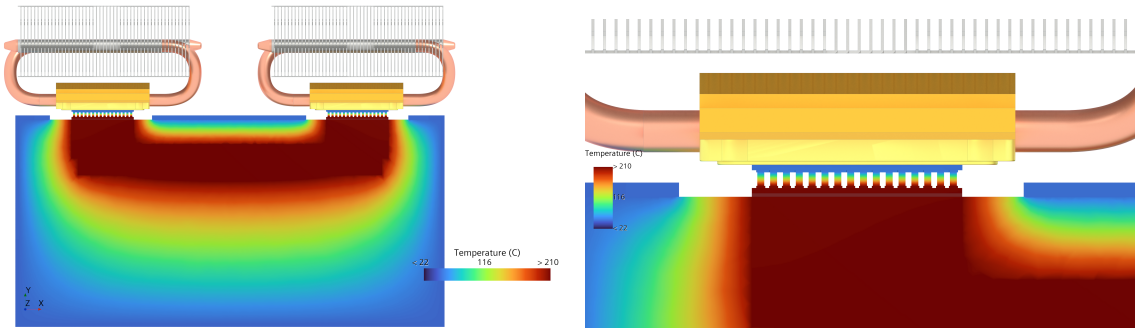

Figure 4. Temperature contours along the midplane of the (top) entire ETG and (bottom) close-up of the TEM.

Table 1. Boundary and interfacial conditions for each region of the computational domain.

Region	Boundary	Condition	Value
Heater element	Internal volume	Heat source	75 W
	Element to sheath	Contact interface	Conformal conduction
Heater sheath	Sheath to element	Contact interface	Conformal conduction
	Sheath to HDB	Contact interface	Conformal conduction
	Sheath to insulation	Contact interface	Conformal conduction
HDB	HDB to sheath	Contact interface	Conformal conduction
	HDB to insulation	Contact interface	Conformal conduction
	HDB to TEM cold shoe	Contact interface	Conformal conduction
TEM shoes	TEM hot shoe to HDB	Contact interface	Conformal conduction
	TEM shoes to interconnects	Contact interface	Conformal conduction
	TEM cold shoe	Thermal specification	50°C
TEM interconnects	Interconnects to TEM hot shoe	Contact interface	Conformal conduction
	Interconnects to TEM cold shoe	Contact interface	Conformal conduction
	Interconnects to TEM legs	Contact interface	Conformal conduction
TEM legs	TEM legs to interconnects	Contact interface	Conformal conduction
Insulation	Insulation to sheath	Contact interface	Conformal conduction
	Insulation to HDB	Contact interface	Conformal conduction
	Insulation to enclosure	Contact interface	Conformal conduction
Enclosure	Enclosure to insulation	Contact interface	Conformal conduction
	Enclosure top	Convective heat transfer	2 $\mathrm{W\,m^{-2}\,K^{-1}}$
	Enclosure sides	Convective heat transfer	5 $\mathrm{W\,m^{-2}\,K^{-1}}$
	Enclosure bottom	Convective heat transfer	1 $\mathrm{W\,m^{-2}\,K^{-1}}$

Table 2. Specified material properties for each region of the computational domain

Component	**Material**	**Density** ($kg\,m^{-3}$)	**Specific heat** ($J\,kg^{-1}\,K^{-1}$)	**Thermal conductivity** ($W\,m^{-1}\,K^{-1}$)
Heater element	MgO[a]	3,580	877	Polynominal
Heater sheath	UNS S30400[b]	8,000	502	Polynominal
Heat distribution block	C110[c]	8,940	386	Polynominal
TEM shoes	Al_2O_3[d]	4,000	900	Polynominal
TEM interconnect bridges	C110[c]	8,940	386	Polynominal
TEM legs	Bi_2Te_3[e]	7,740	154	Polynominal
Insulation	Min-k TE 1400[f]	320	837	Polynominal
Enclosure	Al[g]	2,700	903	Polynominal

[a] MgO thermophysical properties of [13]
[b] UNS S30400 thermophysical properties of [14]
[c] C110 thermophysical properties of [14]
[d] Al_2O_3 thermophysical properties of [15]
[e] Bi_2Te_3 thermophysical properties of [9, 10]
[f] Min-k TE 1400 thermophysical properties of [14]
[g] Al thermophysical properties of [14]

3. DEMONSTRATION UNIT

A demonstration unit was constructed to showcase the ETG'S compact size, versatility, and ability to serve as a power source. The ETG described in Section 2 was installed into a protective case (NANUK 933) for transportation during travel. The small footprint of the ETG allowed for it to be fixed inside the 18 $\times$ 13 $\times$ 9.5 in. (L $\times$ W $\times$ H) case, with extra space remaining for instrumentation and controls. The customized case included a 12 in. touch screen (Automation Direct CM5-T12W), and a programmable logic controller (PLC) (Automation Direct, C0-12DD2E-2-D) with a temperature module (Automation Direct, C0-04THM). The packaged demonstration unit can be seen in Figure 5.

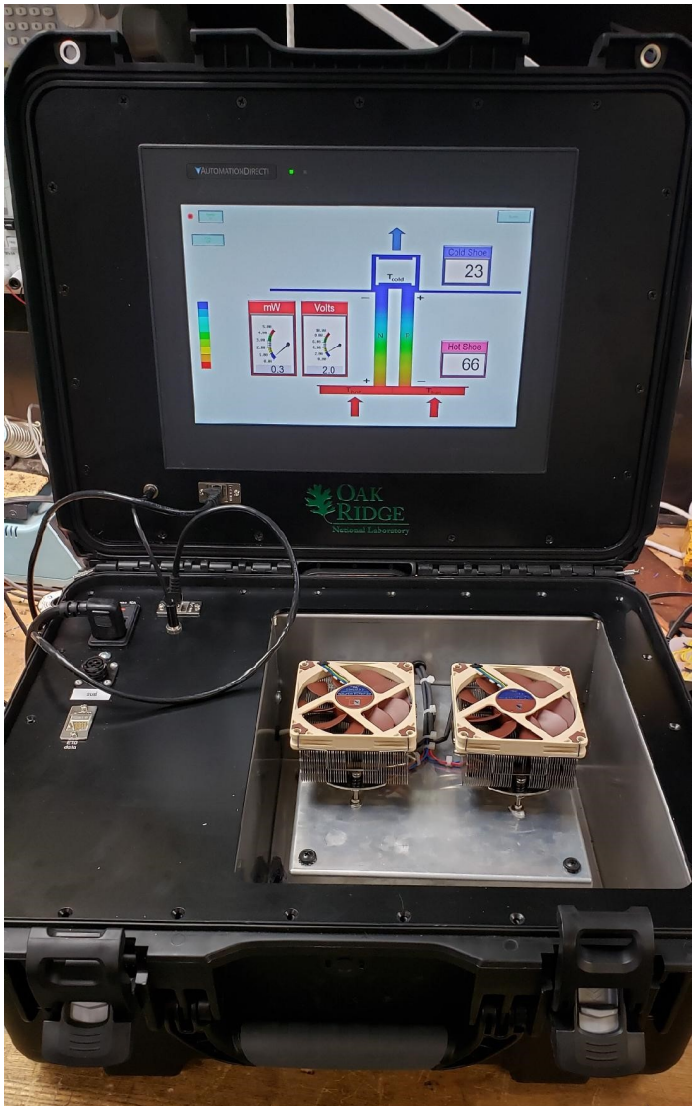

Figure 5. Portable and rugged ETG demonstration unit.

The demonstration unit is supplied with 120 VAC electrical power. A set of power and data cables connect the PLC to the instrumentation modules. A series of screens are available to monitor and control the ETG's temperature, power generation, voltage generation, and current generation. These include line plots versus time, analog gauges, and infographics related to simulation models of the TEMs and entire unit.

The unit is activated by defining a desired temperature set point for the electrical heater. The proportional–integral–derivativ loop is tuned to gradually bring the system up to its maximum operating temperature over 20 min. The automatic heater control eliminates the need for manual intervention during presentations and avoids exceeding the thermal limits of the BiTe TEM solder, which is the limiting component of the unit.

After 10 min, the TEMs begin to generate sufficient voltage and current to drive 12 VDC fans attached to the top of each TEM's heat sink. The activation of these fans significantly decreases the TEM cold shoe temperature and increases the overall ΔT. This further accelerates the rate at which electrical power, voltage, and current are generated until the unit reaches a thermoelectric equilibrium at the desired temperature set point.

A barrel connector port was integrated into the NANUK 933 protective case. When a cord is plugged in, a portion of the ETG electrical power can be diverted to directly powering another device. During demonstrations, an AM submersible with a LiON battery pack is docked with the ETG. After sufficient time, the submersible can be undocked. The potential energy within the LiON battery pack is then directed to a shaft and propeller. Figure 6 presents the AM submersible.

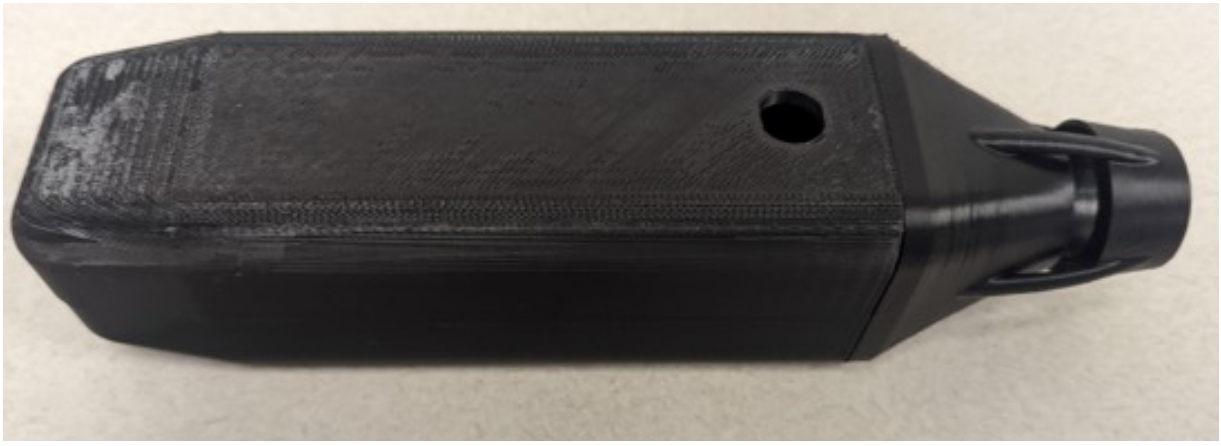

Figure 6. AM submersible that can be docked with the ETG and receive electrical energy generated from the TEM.

4. VALIDATION UNIT

To generate the appropriate data needed to validate the coupled thermal-electric computational model, a second instrumented ETG was constructed. The functional requirements of the validation unit included the ability to do the following:

1. Control, measure, and record the power supplied to the heater.
2. Measure and record temperature response.
3. Vary load resistances on the TEM.
4. Measure and record the TEM output voltage and current.
5. Operate the cooling fans at a constant 12 V and speed.

A Watlow F4T process controller, shown in Figure 7, was selected to serve as the validations unit controller and data logger. A solid-state relay was used to control the strip heater to output a constant power. The heat sink fans were initially connected to a voltage divider from one of the digital outputs of the Watlow controller but led to irregular pulsing of the fan. To maintain a constant fan speed and thus a constant boundary condition, an external power supply (Acopian TD12-100) was deployed.

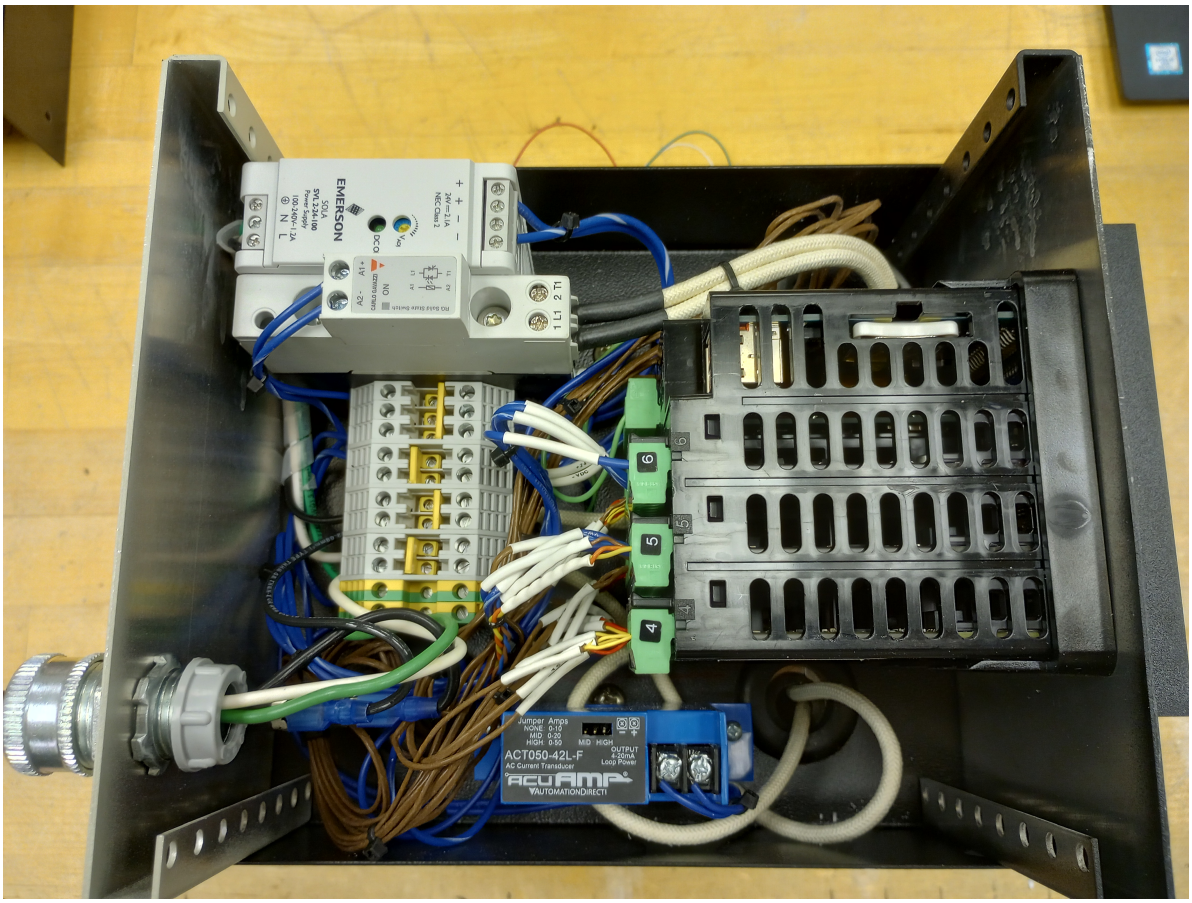

Figure 7. Watlow F4T customized process controllers and data acquisition.

A total of 17 K-type thermocouples were spot welded at multiple locations on the ETG to provide temperature measurements. Figure 8 provides an overview of the thermocouple locations. Figure 9 shows how each thermocouple was spot welded on the surface of the corresponding subcomponent. The ability to capture temperatures across the ETG subcomponents is important for model comparison. Temperatures and TEM voltages were sampled at a rate of 1 Hz.

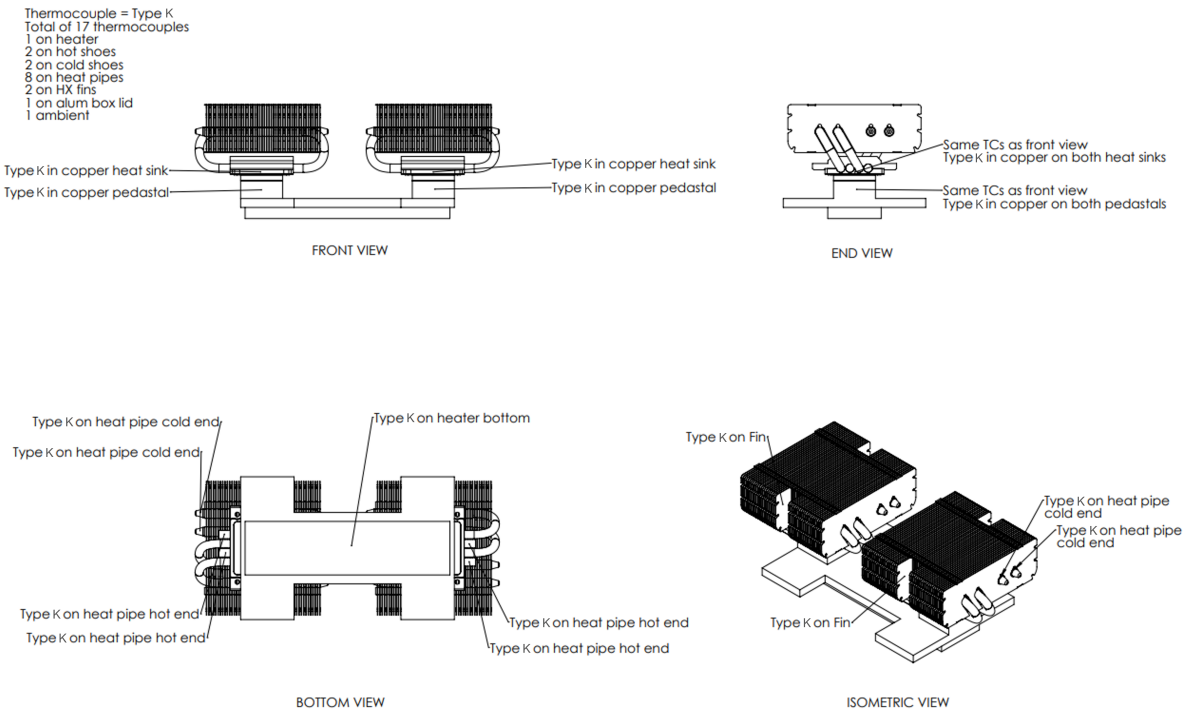

Figure 8. Assembly drawing showing the K-type thermocouple locations.

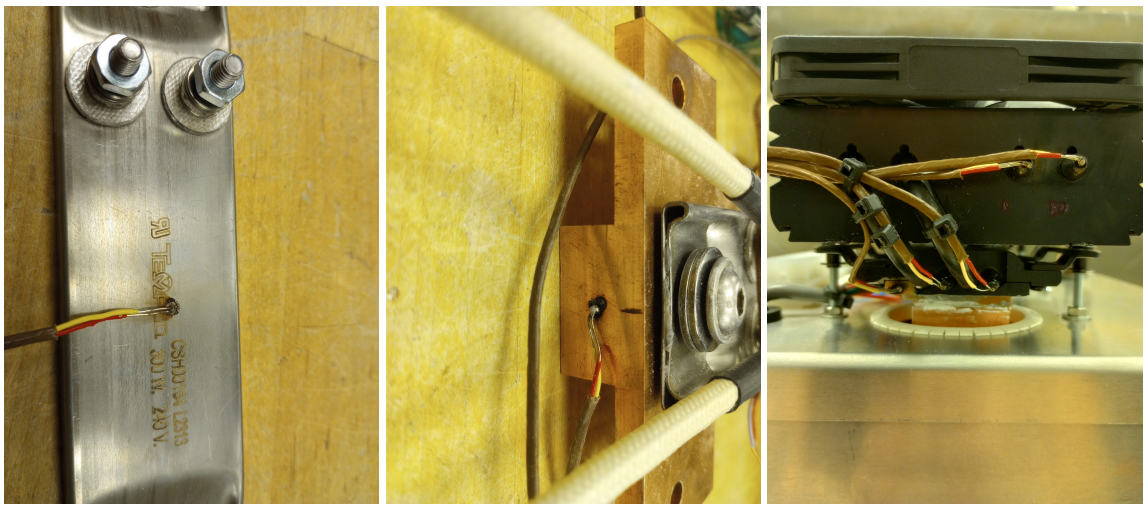

(a) Heater (b) Copper Pedestal (c) Heat Sink

Figure 9. Spot welded thermocouples on subcomponent surfaces.

An electrical bus provided quick access to the TEM wire leads. Figure 10 shows the assembled unit used to generate data for model validation. The external load on the TEM was set using 2 W resistors in series, parallel, and in series/paralle combinations to achieve the desired total circuit resistance. In lieu of a decade box, a standard breadboard was initially used. When conducting tests, careful attention should be given to the resistor connections when integrating into the circuit. Large fluctuations in the TEM output voltage and current were observed when using a breadboard because of poor electrical contact and thermal expansion of the resistor legs. After experiencing such fluctuations, the breadboard was removed and electrical connections were made using more secure lever-nuts to pin the resistor legs. Table 3 provides a typical load resistance sweep that can be performed using the validation unit.

A thermoelectric generator is a tightly coupled system that experiences positively correlated behavior for TEM ΔT and electrical output. There is also a coupled system response where joule heating affects the thermal heat flux and hot and cold shoe surface-averaged temperatures. For example, the validation unit hot shoe temperature can swing 20% at a constant thermal power between the open circuit configuration and a 1 Ω load resistance. Since the load influences the entire ETG system temperature, it is important to ensure equal resistances were applied to both TEMs that were on separate electrical circuits rather than in series. An ammeter (McMaster #8339T3) connected in series with the TEM circuit measured the module's current output as a function of load resistance and operating temperature. The power output of the TEMs can be calculated as $P = IV$, where P is power, I is current, and V is voltage. It is also important to allow the ETG and resistors to reach thermal equilibrium before collecting data for steady-state operation. It was found that 30 min was the minimum time for the unit to stabilize.

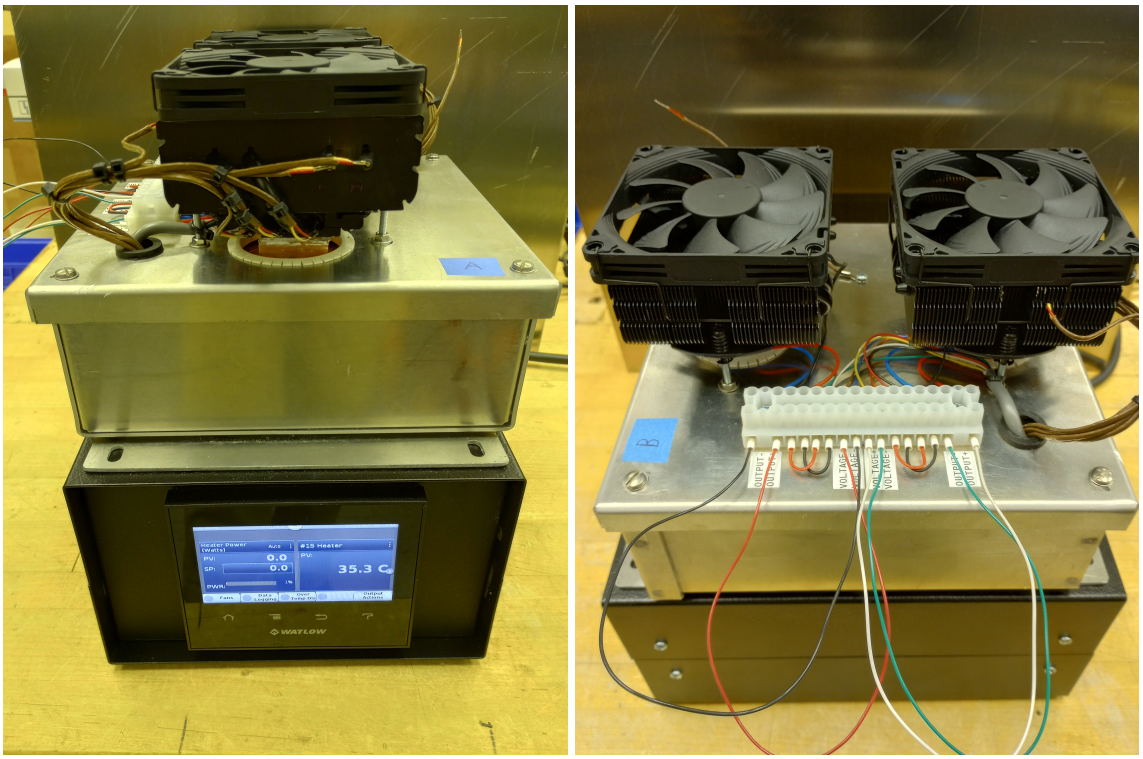

(a) Front view with graphical touch panel

(b) Side view with TEM terminal block

Figure 10. Instrumented ETG validation unit.

Table 3. Load resistance sweep at a constant heater power.

Test #	Heater Power (W)	Load Resistance (Ohms)
1	60	1
2	60	2
3	60	4
4	60	5
5	60	6
6	60	7
7	60	8.28
8	60	9
9	60	10
10	60	11
11	60	12
12	60	14
13	60	17
14	60	20
15	60	25
16	60	30
17	60	35
18	60	40

REFERENCES

[1] T. Hammel, R. Bennett, B. Sievers, Evolutionary upgrade for the multi-mission radioisotope thermoelectric generator (mmrtg), in: 2016 IEEE Aerospace Conference, IEEE, 2016, pp. 1–8.

[2] T. C. Holgate, R. Bennett, L. Renomeron, S. Keyser, I. Chi, J. Ni, K. Yu, T. Caillat, S. Pinkowski, Analysis of raw materials sourcing and the implications for the performance of skutterudite couples in multi-mission radioisotope thermoelectric generators, Journal of Electronic Materials 48 (2019) 7526–7532.

[3] A. Schock, T. Hamrick, V. Sankarankandath, M. Shirbacheh, Design and structural analysis of mars rover rtg, Tech. rep., Fairchild Space Company (1989).

[4] Gphs-rtgs in support of the cassini rtg program. semi annual technical progress report, september 26, 1994–april 2, 1995 (4 1995).

[5] G. L. Bennett, J. J. Lombardo, R. J. Hemler, G. Silverman, C. W. Whitmore, W. R. Amos, E. W. Johnson, R. W. Zocher, J. C. Hagan, R. W. Englehart, The General-Purpose Heat Source Radioisotope Thermoelectric Generator: A Truly General-Purpose Space RTG, AIP Conference Proceedings 969 (1) (2008) 663–671.

[6] H. Carney, An undersea radioisotope power supply (1967).

[7] J. Glenn, J. Patterson, K. DeRoos, J. Patterson, K. Mitchell, L. Strata-G, Disposition of radioisotope thermoelectric generators currently located at the oak ridge national laboratory–12232, in: WM2012, 2012.

[8] C. L. Cramer, H. Wang, K. Ma, Performance of functionally graded thermoelectric materials and devices a review, Journal of Electronic Materials 47 (9) (2018).

[9] H. Wang, W. D. Porter, H. Bottner, J. Konig, L. Chen, S. Bai, T. M. Tritt, A. Mayolet, J. Senawiratne, C. Smith, et al., Transport properties of bulk thermoelectrics—an international round-robin study, part i seebeck coefficient and electrical resistivity, Journal of electronic materials 42 (2013) 654–664.

[10] H. Wang, W. D. Porter, H. Bottner, J. Konig, L. Chen, S. Bai, T. M. Tritt, A. Mayolet, J. Senawiratne, C. Smith, et al., Transport properties of bulk thermoelectrics: an international round-robin study, part ii thermal diffusivity, specific heat, and thermal conductivity, Journal of electronic materials 42 (2013) 1073–1084.

[11] I. Hrbud, K. Goodfellow, M. Van Dyke, M. Houts, Non-nuclear nep system testing, AIP Conference Proceedings 654 (1) (2003) 533–539.

[12] M. H. Briggs, M. A. Gibson, J. L. Sanzi, Electrically heated testing of the kilowatt reactor using stirling technology (krusty) experiment using a depleted uranium core, in: AIAA Propulsion and Energy Forum and Exposition, no. NASA/TM-2018-219702, 2018.

[13] A. J. Slifka, B. J. Filla, J. Phelps, Thermal conductivity of magnesium oxide from absolute, steady-state measurements, Journal of Research of the National Institute of Standards and Technology 103 (4) (1998) 357.

[14] K. C. Mills, Recommended values of thermophysical properties for selected commercial alloys, Woodhead publishing, 2002.

[15] Y. Touloukian, Recommended values of the thermophysical properties of eight alloys, major constituents and their oxides, february 1, 1965-january 31, 1966, Tech. rep. (1966).

APPENDIX A. ASSEMBLY PROCESS

APPENDIX A. ASSEMBLY PROCESS

The enclosed insulated ETG was assembled as follows:

1. The aluminum enclosure side walls were cut to 4 in.
2. The min-k insulation was machined to accept the copper block and heater terminals.
3. The enclosure was insulated as shown in Figure 2.
4. Alignment was checked between the heater slots and the tapped holes in the copper heat distribution block.
5. Electrical wired strip heater using 450°C high-temperature wire.
6. Applied boron nitride thermal paste evenly on strip heater.
7. Bolts from 5/16–8 in., Belleville conical washers, and regular washers were used to mount the heater to the copper block.
   (a) A stack of two washers was needed to clear the heater sheath.
   (b) The bolt near the wire terminals was fully tightened (15 ft·lb).
   (c) The bolt opposite the wire terminals was left loose (1/4 in. turn past hand tight).
8. Two 2 in. holes and four 1/4 in. holes aligned with the heat distribution block were punched in the aluminum enclosure lid.
9. The underside of the enclosure lid was insulated.
10. The copper block, TEMs, heat sinks, and aluminum lid were stacked and pressed together using the heat sink screws and the copper block tabs.
    (a) Boron nitride thermal paste was evenly applied to the TEM's **hot** shoe side and placed on copper pedestals.
    (b) Noctua HT-H1 thermal paste was evenly applied to the TEM's **cold** shoe side.
    (c) The pedestals were aligned with the enclosure lid before placing heat sinks on the TEM's cold shoe side.
    (d) The TEMs were compressed between the copper pedestals and heat sinks using four M3.5 × 40 mm with small conical Belleville washers and ceramic spacers on the copper tabs.
11. The ETG and lid were mounted to the enclosure.
12. Flexible insulation was used to reduce heat losses from the punched lid holes.